Francisco Mesa, Guido Valerio, Raúl Rodríguez-Berral, and Oscar Quevedo-Teruel

Simulation-Assisted Efficient Computation of the Dispersion Diagram of Periodic Structures

A comprehensive overview with applications to filters, leaky-wave antennas and metasurfaces.

A hybrid method that combines the results of a commercial simulator with analytical postprocessing is discussed and used to compute the dispersion diagrams of periodic structures. The method takes advantage of the ability of commercial simulators to deal with arbitrary geometries and materials and overcomes some of their limitations to compute the attenuation constant. The frequency behavior of the attenuation constant is very valuable for microwave and antenna design because it provides key information on the isolation/rejection in stopbands and the radiation losses in periodic leaky-wave antennas (LWAs). A comprehensive overview of different theoretical and practical issues regarding the computation of dispersion diagrams is first carried out. Important considerations and main assumptions concerning

Digital Object Identifier 10.1109/MAP.2020.3003210
Date of current version: 14 August 2020

©SHUTTERSTOCK.COM/BOBNEVV

Authorized licensed use limited to: Universidad de Sevilla. Downloaded on June 28,2022 at 11:08:41 UTC from IEEE Xplore. Restrictions apply.

the practical implementation of the method and its interaction with the commercial simulator are thoroughly discussed.

INTRODUCTION

The knowledge of the dispersion diagrams of periodic structures is of capital relevance in the general study of wave propagation [1]–[3]. These diagrams provide insight into the behavior and interaction of the waves with the waveguiding environment: the forward/backward and fast/slow wave nature, the level of anisotropy and dispersion, the existence and characteristics of bandgaps, the wave attenuation due to radiation or losses, and so on. Assuming a time-harmonic dependence of the fields, the wave propagation in a 1D periodic structure along the direction of periodicity can mathematically be solved with a Floquet analysis. This means that the potentials/fields in the structure, denoted here in general as $\mathbf{C}$, satisfy the following condition [2]:

$$\mathbf{C}(x,y,z,t) = \mathbf{C}_p(x,y,z)\,\mathrm{e}^{-\gamma z}\,\mathrm{e}^{\mathrm{j}\omega t}, \tag{1}$$

where ω is the angular frequency, $\gamma\,(\equiv \mathrm{j}k_z) = \alpha + \mathrm{j}\beta$ is the complex propagation constant along the assumed wave-propagation direction (z), with α being the attenuation constant and β the phase constant ($k_z = -\mathrm{j}\gamma = \beta - \mathrm{j}\alpha$ is the complex wavenumber along the z-direction). The periodic function $\mathbf{C}_p$ satisfies $\mathbf{C}_p(x,y,z) = C_p(x,y,z+np)$, with np being an integer multiple of the period of the structure. Starting from the general condition (1), the dispersion relations of periodic guiding/radiating electromagnetic (EM) structures have been computed with a large variety of methods. Following [4], these methods can be classified into two categories: 1) methods that compute the propagation constant at each frequency and 2) methods that extract the frequency at which the unit cell of the periodic structure resonates when subject to a given phase shift along the periodicity direction.

One key issue that complicates any of the possible solution methods is the complex nature of the propagation constant (having both imaginary and real parts), which may occur for both bounded and unbounded waveguiding systems, even in the absence of material losses. However, there is an important difference between the modal solutions of bounded and unbounded guiding structures. Bounded waveguiding systems, shielded by either electric/magnetic walls or periodic boundary conditions, always lead to wave equations that can be framed into the so-called Sturm–Liouville problems of the first kind [5]. Their modal analysis always yields eigenvalue problems with a discrete spectrum [2], [5] whose possible solutions are bound, evanescent, and complex modes [2], [6]–[8]. When other types of boundary conditions and/or unbounded regions are present in the waveguiding system, the spectrum of the resulting eigenproblem has both continuous and discrete parts. As the continuous spectrum of any EM problem can be partly associated with the power radiated to the unbounded region [2], [5], complex, leaky-wave modal solutions can now appear in the dispersion relation of the structure [2], [9], [10]. In general, the appearance of modes with complex propagation constants means that the solution of the modal characteristic equation requires extra mathematical and numerical tasks [2], [7], [10]. Scientific literature shows that a lot of effort has been devoted to finding appropriate methods for searching for the complex roots of the characteristic equations, or, directly, to avoid such root searching.

The knowledge of the dispersion diagrams of periodic structures is of capital relevance in the general study of wave propagation.

Today, a very common practice is the use of commercial full-wave simulators (HFSS, CST, FEKO, ADS, and so on) in the analysis and/or design of microwave and antenna devices. Certainly, the ability of these simulators to deal with very general structures is one of their most appreciated assets. The price to pay for this wide applicability is their often elevated demand of computational and memory resources. Concerning the calculation of dispersion diagrams, to the best of our knowledge, existing simulators do not compute the complete dispersion diagram of all the modal solutions of periodic waveguiding systems but rather only the behavior of the phase shift (β_p) versus frequency and the attenuation constant due to material losses. However, the information of the attenuation constant is crucial for many lossless and radiating cases, especially in EM bandgap structures as well as in LWAs.

In this article, we present a thorough discussion on how the so-called multimode transfer-matrix method [2], [4], [11]–[19] combines the simulator's advantage of dealing with a wide range of material and arbitrarily shaped structures together with convenient postprocessing to compute the complete dispersion diagram of periodic structures. With this method, one can obtain the information of the modal-attenuation constant, regardless whether it comes from either losses, radiation, or the intrinsic complex/evanescent nature of the modes. Different novel aspects of the application of the method to unbounded radiative structures as well as 2D configurations are considered. Additionally, the presence of higher symmetries in the unit cell is also contemplated.

ANALYSIS

To keep the discussion and analysis in this section as simple as possible, only 1D periodicity will be considered. The extension to 2D periodic structures is addressed later in the "2D Periodic Structures" section.

EIGENPROBLEMS IN GUIDED-WAVE ANALYSIS

Before discussing the periodic case, some of the main features of the uniform (nonperiodic) problem in the frequency domain are briefly outlined.

UNIFORM STRUCTURES

In this situation, we have a structure invariant to arbitrary translations along the propagating z-direction, as shown in Figure 1(a). Regardless of the employed method of analysis, the

Authorized licensed use limited to: Universidad de Sevilla. Downloaded on June 28,2022 at 11:08:41 UTC from IEEE Xplore. Restrictions apply.

procedure used to find the modes of the structure [2], [20] will lead to an eigenproblem that can be expressed, in general, as

$$[\mathbf{\Gamma}(k_z,\omega)]\,\mathbf{u} = 0, \tag{2}$$

where k_z are the eigenvalues (modal wavenumbers) of the problem, $\mathbf{u}$ are the corresponding eigenvectors, and $[\mathbf{\Gamma}]$ is the matrix associated with the projection method employed to solve the corresponding full-wave Floquet-periodic problem, for instance, method of moments [21], the finite-element method [22], mode matching [23], the Nystrom collocation method [24], and so on. It should be noted that, in general, the aforementioned eigenproblem is nonlinear and, only under certain circumstances (for instance, the case of a homogeneous rectangular waveguide) does it turn into a linear eigenproblem [25]. The boundary integral resonant mode expansion method reported in [26] provides a procedure to linearize the eigenproblem for homogeneous waveguides with an arbitrary shape. Notwithstanding, the dispersion relation of the structure can always be expressed as the solution of

$$F(k_z;\omega) \equiv \det\{[\mathbf{\Gamma}(k_z,\omega)]\} = 0. \tag{3}$$

For each value of frequency ω, the solution of (3) means searching for the complex zeros of complex function $F(k_z)$. In general, this zero searching is not simple, as it is one of the recurrent problems in the literature on modal analysis [27]–[31]. The two main reasons why it is difficult to search numerically for complex zeros are 1) the functions have poles and branch-point singularities and 2) it is difficult to find a systematic and reliable algorithm that can explore the complex plane, which can comprise several Riemann sheets, without losing any of the zeros of the function. Possibly because of these two underlying drawbacks, most commercial simulators avoid this zero searching and do not usually provide the complete dispersion relation of uniform structures.

PERIODIC STRUCTURES

If the modal analysis is to be applied to 1D periodic structures (periodicity along the propagating z-direction), as shown in Figure 1(b), the solution of the corresponding full-wave Floquet-periodic problem also leads, in general, to a nonlinear eigenvalue problem [32]. This means that the same difficulties involved with obtaining the dispersion relation of uniform structures also hold for 1D periodic structures. Because of this, many efforts have been devoted to circumventing this problem, and different alternatives have been reported in the literature to formulate an equivalent linear eigenproblem.

One possibility is to solve, directly, Maxwell's equations in the time domain. Examples of this procedure are the finite difference time domain (FDTD) methods reported, such as in [33]–[36]. The approaches presented in [33] and [34] dealt with only real propagation constants, but the possibility of losses/radiation was successfully incorporated in [35] and [36]. Although these time-domain methods avoid the difficult task of searching for complex zeros, their intrinsic iterative nature involves very large, sometimes sparse, matrices. This usually leads to intensive computational efforts and high demands of storage apart from the numerical instabilities that may appear when nonuniform grid meshing is required to deal with complex geometries as well as multiscale structures. Similar problems can also be found in the finite difference frequency domain (FDFD) method reported in [4]. Enhanced implementations of FDTD and FDFD methods can partially alleviate some of the aforementioned problems, but this issue is beyond the scope of the present work which is more focused on frequency-domain IE methods.

Another common approach used to find the dispersion diagram as the solution of a linear eigenproblem is to model the 1D periodic structure as a two-port equivalent network characterized by its transfer (ABCD) matrix [**T**] and subject to periodic boundary conditions along the propagation direction [2], [25]. Next, two different implementations of this method will be briefly outlined before discussing a third method that can overcome most of the limitations of the previous two.

METHOD 1-UC: TWO-PORT TRANSFER MATRIX OF A SINGLE UNIT-CELL

One of the most common and simple strategies consists of describing the periodic structure, which is invariant under translations of an integer multiple of periods, as a housing waveguide loaded by some additional periodic elements (or discontinuities). The housing waveguide is uniform (i.e., invariant with respect to an arbitrary translation) and would support a certain number of modes in the absence of any periodic load. A transfer matrix [**T**] can then be associated with a single unit-cell of the periodic structure, excited at its access ports by the fundamental mode of the housing waveguide, as shown in Figure 2(a). For instance, in the unit cell shown in Figure 1(b), the housing waveguide is a microstrip line and the "discontinuities" are the lateral metallic stubs placed on both sides of the conducting strip. Although such a distinction between the housing waveguide and its discontinuity is difficult in some structures, in principle, this decomposition can always be done. In this first simplified method, the original 1D periodic EM problem can be modeled as a cascade of the two-port transfer matrices, as depicted in Figure 2(b), where the actual transfer matrix $[\mathbf{T}_p]$ of the unit cell within the periodic environment is assumed to be given by the transfer matrix [**T**] of the single unit-cell taken isolated, i.e., $[\mathbf{T}_p] \approx [\mathbf{T}]$. It is worth pointing out the difference between the so-called [**T**] and $[\mathbf{T}_p]$ matrices. The [**T**] matrix corresponds to the transfer matrix of an isolated, single unit-cell as shown in Figure 2(a), whereas the $[\mathbf{T}_p]$ matrix stands for the transfer matrix

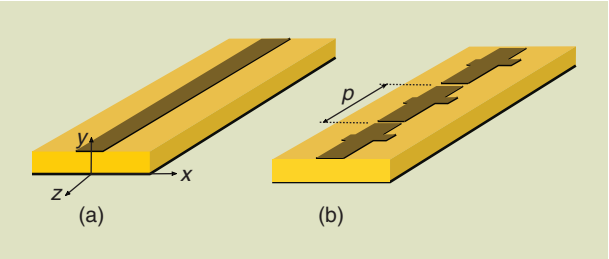

FIGURE 1. Examples of (a) the uniform waveguiding system and (b) the 1D periodic structure of period p.

Authorized licensed use limited to: Universidad de Sevilla. Downloaded on June 28,2022 at 11:08:41 UTC from IEEE Xplore. Restrictions apply.

of the unit cell when it is part of the infinitely periodic structure. In principle, this last matrix cannot directly be obtained with a commercial simulator because the simulator can only deal with truncated finite structures having input/output ports.

Often, the discontinuities inside the unit cell can be well characterized by equivalent networks of reactive elements, which are known in closed form [37], [38]. In this simplified situation, the transfer matrix of the single unit-cell is easily computed from the transfer matrices that account for the fundamental-mode propagation in two housing-waveguide sections and the one corresponding to the discontinuity network. In more complex cases, the transfer matrix of the single unit-cell at each frequency can be numerically obtained with the help of commercial simulators. Once the 2×2 transfer matrix $[\mathbf{T}]$ of the single unit-cell

$$[\mathbf{T}] = \begin{bmatrix} A & B \\ C & D \end{bmatrix}, \tag{4}$$

is obtained, the following eigenproblem is reached after applying a Floquet's analysis to solve for the complex propagation constant γ of the infinite periodic structure [2], [3], [25]:

$$[\mathbf{T}]\,\mathbf{u} = e^{\gamma p}\,\mathbf{u}. \tag{5}$$

The $\mathbf{u}$ column matrix 2×1 is given by

$$\mathbf{u} = \begin{bmatrix} V \\ I \end{bmatrix}, \tag{6}$$

with V and I being the voltage and current, respectively, at the output port of the unit-cell problem. Under the assumption of reciprocity, the dispersion relation of the structure is then given by the following well-known expression [25, eq. (8.7)]:

$$\cosh(\gamma p) = \frac{A(\omega) + D(\omega)}{2}, \tag{7}$$

where the frequency dependence of the transfer-matrix entries is explicitly shown.

In the aforementioned simple procedure, at first sight, it may seem that the dispersion relation of the structure has been found by eluding the zero-searching problem intrinsic to the nonlinear eigenproblem associated with any general modal analysis. It should be noted, however, that the solution of the transfer matrix of a single unit-cell via the 3D full-wave commercial simulator has actually required a modal analysis of the input/output port; namely, the fundamental mode of the housing waveguide has previously been obtained. Only after this nonlinear eigenproblem has been internally solved by the simulator is it possible to compute the transfer matrix that leads to the linear eigenproblem in (5). A somewhat similar procedure is reported in [39], where a linear eigenvalue problem is solved after the corresponding integral equation. Other additional relevant issues and approximations implicit in the aforementioned procedure are given next [40].

DRAWBACKS

1) Because only the fundamental mode of the housing waveguide is considered in the analysis and implicitly assumed through the approximation $[\mathbf{T}_p] \approx [\mathbf{T}]$, the interactions between different unit cells supported by high-order modes (HOMs) of the housing waveguide are completely left out. This assumption is no longer valid when the electric size of the period is small as well as in many other practical situations that actually require accounting for the high-order interactions between cells [2, Sec. 9.7].
2) If the housing waveguide is unbounded (for instance, a microstrip line without a top cover), then only the discrete spectrum [2] of the housing waveguide is considered. This condition is intrinsically imposed by the commercial simulators when modeling the input and output ports as waveguiding systems that are bounded by either electric, magnetic, or periodic boundary conditions. As mentioned previously, these boundary conditions always lead to discrete spectra. Thus, when the housing waveguide is unbounded, there is always an implicit detrimental approximation due to the different nature of the spectrum of the input/output ports and the one of the housing waveguide, which are occasionally enhanced by their possible mismatches. Although this drawback may hardly be relevant in many practical circumstances when dealing with bounded fields in open structures, the appropriate characterization of the reflected/transmitted power when radiation is present

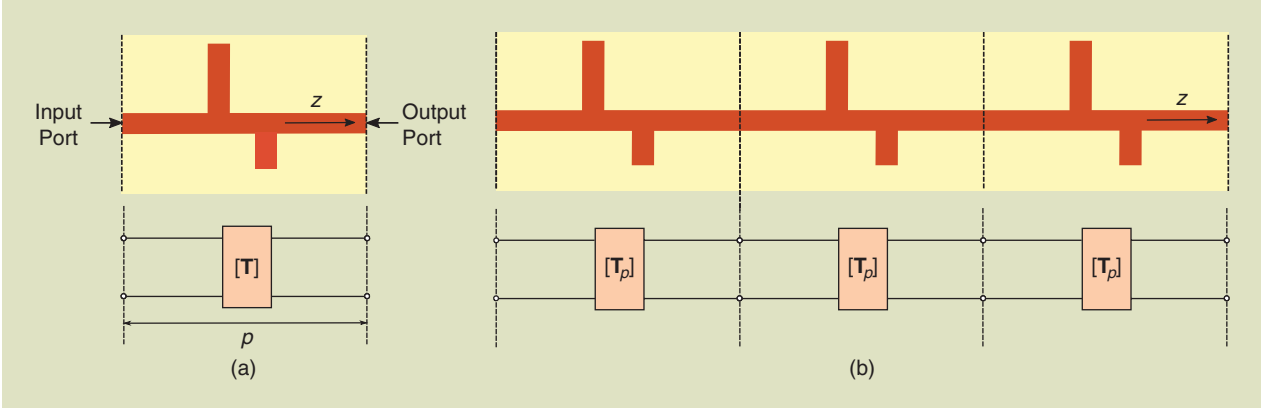

FIGURE 2. (a) The top view of a single cell whose transfer matrix $[\mathbf{T}]$ is to be obtained. (b) The cascade of $[\mathbf{T}_p]$ matrices in the infinite structure. In method 1-uc, it is assumed that $[\mathbf{T}_p] \approx [\mathbf{T}]$.

Authorized licensed use limited to: Universidad de Sevilla. Downloaded on June 28,2022 at 11:08:41 UTC from IEEE Xplore. Restrictions apply.

would require a more careful choice of the input/output ports. In these circumstances, one possible solution could be to ensure that additional variations in the height of the ports do not affect the results of the scattering parameters. More discussions about this issue will be further conducted when the numerical examples are examined in the "Results" section.

METHOD N-UC: TWO-PORT TRANSFER MATRIX OF N UNIT CELLS

In principle, to our knowledge, not much can be done to circumvent drawback 2 from the section "Drawbacks," when significant although possible alternatives involving the development of the in-house, full-wave eigenmode solver have been proposed in [41] and [42]. However, different solutions involving commercial simulators have been reported to overcome drawback 1 [43]–[46]. A common procedure, graphically sketched in Figure 3(a) and (b), is to consider a finite system of multiple unit-cells, say, N, and assume that the two-port transfer matrix of this N-cell system, $[\mathbf{T}_N]$, is related to the transfer matrix of the unit cell in the periodic environment as follows [47]:

$$[\mathbf{T}_p] = \sqrt[N]{[\mathbf{T}_N]}\,. \tag{8}$$

Drawbacks 1 and 2 are still present at the two ports of the N-cell system. Nevertheless, they are partially mitigated by the computation of the coupling between the unit cells inside the system because the inner boundaries between cells are no more described by equivalent bounded and monomodal ports. It is this fact that is expected to improve the precision of the mutual interactions among the cells as N increases. Still, numerical problems also affect this procedure [47]. Among them is the eventual high computational cost associated with analyzing a finite structure with many cells, which can easily lead to numerical noise and inaccuracies. Another relevant problem comes from the inherent ambiguity in the propagation-constant solutions of the N-cell problem because of the nonuniqueness of the Nth root of a complex number. This leads to an ambiguity on the value of the phase constant, which needs to be addressed (e.g., as in [47]). Furthermore, the case of an LWA that required many unit cells to accurately characterize its complex propagation constant but with a nonsmall radiation attenuation could pose an important numerical problem due to the nearly negligible values of the field at the output port of the N-cell structure.

PROPOSED METHODOLOGY

A methodology that can overcome most of the aforementioned drawbacks is discussed in this section. First, it should be mentioned that the main limitation of the frequency-domain eigenmode solver of commercial simulators comes from the difficulties associated with providing the complex modal-attenuation constants of periodic structures, regardless whether the losses come from either the evanescent/complex nature of the modes or from the presence of unbounded/lossy regions in the periodic structure. Nevertheless, it is apparent that commercial simulators can deal efficiently with unbounded/lossy structures with regard to the computation of the scattering parameters of such structures.

1D PERIODIC STRUCTURES

For the simpler case of 1D periodic structures, the corresponding transfer matrix of an isolated unit cell can be easily obtained from the scattering matrix of the structure modeled as a two-port network [25]. However, as previously discussed in the "Periodic Structures" section, the use of a two-port transfer matrix also brings some drawbacks. Hence, similar to [2], [4], and [11]–[18], it is proposed to continue using the transfer matrix of a single unit-cell of the periodic structure but extend its capabilities by modeling this unit cell as a multiport transfer matrix that takes into account multiple modes of the structure. A graphical representation of this procedure is shown in Figure 3(c). In doing so, the intercell coupling effect due to HOMs can now be well accounted for, an effect that method 1-uc in the "Method 1-UC: Two-Port Transfer Matrix of a Single Unit-Cell" section could not take into account. Very often, the use of multiport equivalent networks is associated with the actual presence of more than two physical ports (terminals) in the structure [15], [48]. However, it is well known that this requirement is not necessary, and the ports can be equally associated with the different modes (propagative, evanescent, and so on) of a structure with just one input and one output physical terminal [2], [3], [37].

For a multiport (or multimode) system, the transformation from the scattering matrix [49], [50] to the transfer matrix [51] is not direct, but it can be easily carried out once the input and output ports of the structure are clearly defined. For this

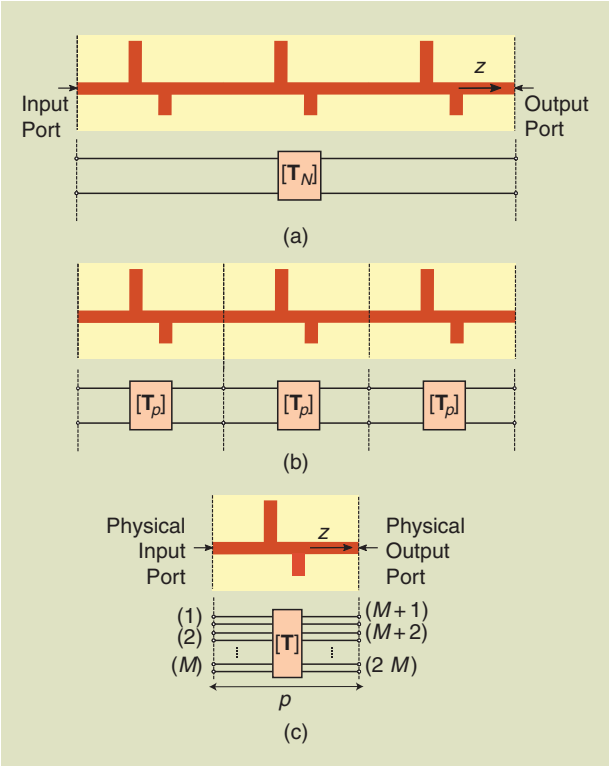

FIGURE 3. (a) The top view of a N-cell structure whose transfer matrix $[\mathbf{T}_N]$ is to be obtained. (b) The cascade of $[\mathbf{T}_p]$ matrices in the infinite structure. In method N-uc, it is assumed that $[\mathbf{T}_p] \approx \sqrt[N]{[\mathbf{T}_N]}$. (c) The finite structure with a single unit-cell whose HOM transfer matrix $[\mathbf{T}]$ is to be obtained.

Authorized licensed use limited to: Universidad de Sevilla. Downloaded on June 28,2022 at 11:08:41 UTC from IEEE Xplore. Restrictions apply.

purpose, let us consider a balanced $2M$-port system whose input ports are numbered $1, 2, \ldots, M$, corresponding to the first M-significant modes, and output ports $M+1, \ldots, 2M$ [see Figure 3(c) associated with the same set of significant modes]. To find the multiport (multimode) transfer matrix, the scattering matrix is written in terms of four partitioned submatrices as

$$[\mathbf{S}] = \begin{bmatrix} [\mathbf{S}_{ii}] & [\mathbf{S}_{io}] \\ [\mathbf{S}_{oi}] & [\mathbf{S}_{oo}] \end{bmatrix}, \tag{9}$$

where subscripts i and o stand for the input and output ports, respectively, and each submatrix corresponds to the generalized scattering matrix that relates the input/output M modes. The multiport (multimode) transfer matrix can be obtained following, for instance, the derivations reported in [51] and [52]. Alternatively, some relatively simple algebraic operations lead us to the following expressions for the block-matrix elements of the transfer matrix:

$$[\mathbf{T}] = \begin{bmatrix} [\mathbf{A}] & [\mathbf{B}] \\ [\mathbf{C}] & [\mathbf{D}] \end{bmatrix}, \tag{10}$$

where

$$[\mathbf{A}] = \frac{1}{2}\big[([\mathbf{1}] + [\mathbf{S}_{ii}])[\mathbf{S}_{oi}]^{-1}([\mathbf{1}] - [\mathbf{S}_{oo}]) + [\mathbf{S}_{io}]\big], \tag{11}$$

$$[\mathbf{B}] = \frac{1}{2}\big[([\mathbf{1}] + [\mathbf{S}_{ii}])[\mathbf{S}_{oi}]^{-1}([\mathbf{1}] + [\mathbf{S}_{oo}]) - [\mathbf{S}_{io}]\big][\mathbf{Z}_o], \tag{12}$$

$$[\mathbf{C}] = \frac{1}{2}[\mathbf{Z}_i]^{-1}\big[([\mathbf{1}] - [\mathbf{S}_{ii}])[\mathbf{S}_{oi}]^{-1}([\mathbf{1}] - [\mathbf{S}_{oo}]) - [\mathbf{S}_{io}]\big], \tag{13}$$

$$[\mathbf{D}] = \frac{1}{2}[\mathbf{Z}_i]^{-1}\big[([\mathbf{1}] - [\mathbf{S}_{ii}])[\mathbf{S}_{oi}]^{-1}([\mathbf{1}] + [\mathbf{S}_{oo}]) + [\mathbf{S}_{io}]\big][\mathbf{Z}_o], \tag{14}$$

with $[\mathbf{1}]$ being the $M \times M$ identity matrix and $[\mathbf{Z}_i]$ and $[\mathbf{Z}_o]$ the square matrices whose diagonal elements are the input/output characteristic port impedances, namely,

$$[\mathbf{Z}_{i/o}] = [\mathrm{diag}(Z_{i/o,m})]. \tag{15}$$

An interesting question that arises here is that the specific values of the impedances of the ports do not have any effect on the eigenvalues of the multiport transfer matrix as long as the same value is employed for the same mode at the input and output ports (that is, if $[\mathbf{Z}_i] = [\mathbf{Z}_o]$). This can be easily observed by rewriting the $[\mathbf{T}]$ matrix as

$$[\mathbf{T}] = \begin{bmatrix} [\mathbf{1}] & [\mathbf{0}] \\ [\mathbf{0}] & [\mathbf{Z}_i]^{-1} \end{bmatrix}[\mathbf{T}_1]\begin{bmatrix} [\mathbf{1}] & [\mathbf{0}] \\ [\mathbf{0}] & [\mathbf{Z}_o] \end{bmatrix}, \tag{16}$$

where $[\mathbf{T}_1]$ stands for the transfer matrix defined with unitary port impedances, and $[\mathbf{0}]$ stands for the $M \times M$ null matrix. As long as $[\mathbf{Z}_i] = [\mathbf{Z}_o]$, $[\mathbf{T}]$ is similar to $[\mathbf{T}_1]$ for any choice of the port impedances, its eigenvalues are then invariant under a change of the impedances.

Assuming now that the aforementioned multimode $[\mathbf{T}]$ matrix is a good approximation of the multimode transfer matrix of the unit cell in the periodic environment, the eigenproblem to be solved is [2], [11], [12], and [15]–[19]

$$[\mathbf{T}]\begin{bmatrix} \mathbf{V} \\ \mathbf{I} \end{bmatrix} = \mathrm{e}^{\gamma p}\begin{bmatrix} \mathbf{V} \\ \mathbf{I} \end{bmatrix}, \tag{17}$$

where $\mathbf{V}$ and $\mathbf{I}$ are now $M \times 1$ arrays containing the voltages and currents, respectively, at the output ports. This eigenproblem is formally identical to (5) for the two-port case. The only relevant difference is that we will find M pairs of eigenvalues associated with $\pm\gamma_m p$ $(m = 1, \ldots, M)$.

If the unit cell under study is reciprocal, the inverse of the transfer matrix satisfies [51, eq. (51)]

$$[\mathbf{T}]^{-1} = \begin{bmatrix} [\mathbf{D}]^T & -[\mathbf{B}]^T \\ -[\mathbf{C}]^T & [\mathbf{A}]^T \end{bmatrix}, \tag{18}$$

where superscript T means transpose. For this matrix, the following eigenvalue problem holds:

$$[\mathbf{T}]^{-1}\begin{bmatrix} \mathbf{V} \\ \mathbf{I} \end{bmatrix} = \mathrm{e}^{-\gamma p}\begin{bmatrix} \mathbf{V} \\ \mathbf{I} \end{bmatrix}. \tag{19}$$

Summing eigenproblems (17) and (19) for the multimode- and inverse-transfer matrices, the following eigenvalue problem is obtained:

$$\begin{bmatrix} [\mathbf{A}] + [\mathbf{D}]^T & [\mathbf{B}] - [\mathbf{B}]^T \\ [\mathbf{C}] - [\mathbf{C}]^T & [\mathbf{D}] + [\mathbf{A}]^T \end{bmatrix}\begin{bmatrix} \mathbf{V} \\ \mathbf{I} \end{bmatrix} = 2\cosh(\gamma p)\begin{bmatrix} \mathbf{V} \\ \mathbf{I} \end{bmatrix}, \tag{20}$$

which turns out to have two degenerate set of eigenvalues; namely, each $\gamma_m p$ is a double solution of (20). If the structure is also symmetric, then $[\mathbf{A}] = [\mathbf{D}]^T$, $[\mathbf{B}] = [\mathbf{B}]^T$, and $[\mathbf{C}] = [\mathbf{C}]^T$ [51]. This means that the aforementioned 2 M-rank eigenproblem can be reduced to the M-rank one given by

$$[\mathbf{A}]\mathbf{V} = \cosh(\gamma p)\mathbf{V}. \tag{21}$$

The aforementioned eigenproblem clearly simplifies to the well-known dispersion relation provided in (7) for the simplest case of a two-port symmetric periodic structure.

An interesting practical situation arises if the unit cell under study has any kind of internal higher symmetry (for instance, glide [53] or twist [54] symmetries). In this case, the eigenvalue problem can be set up for the so-called subunit cell (the size of which will be denoted as $\hat{p}$) where the corresponding higher symmetry operator plays the same role as does the Floquet translation-symmetry operator for a standard periodic structure [19], [39], [53], [55]. The resulting generalized eigenvalue problem can then be written, following the notation in [19] and [55], as

$$[\hat{\mathbf{T}}]\begin{bmatrix} \mathbf{V} \\ \mathbf{I} \end{bmatrix} = \mathrm{e}^{\gamma\hat{p}}\begin{bmatrix} [\mathbf{Q}] & [\mathbf{0}] \\ [\mathbf{0}] & [\mathbf{Q}] \end{bmatrix}\begin{bmatrix} \mathbf{V} \\ \mathbf{I} \end{bmatrix}, \tag{22}$$

where $[\hat{\mathbf{T}}]$ is the corresponding multimode transfer matrix for the subunit cell, and $[\mathbf{Q}]$ is a submatrix that accounts for the corresponding algebraic operations resulting from the effects of the specific higher symmetry on the electric/magnetic fields (see "Unit Cells With Higher Symmetries" and [19] and [55]). Dealing directly with the eigenvalue problem in (22) leads to numerical and accuracy advantages because it considerably reduces the size of the structure to be analyzed with the full-wave simulator. If the system is reciprocal and symmetric, the eigenvalue problem can be further simplified [analogous to (21)] into

$$[\hat{\mathbf{A}}]\mathbf{V} = \frac{1}{2}\{e^{\gamma\hat{p}}[\mathbf{Q}] + e^{-\gamma\hat{p}}[\mathbf{Q}]^{-1}\}\mathbf{V}. \tag{23}$$

Authorized licensed use limited to: Universidad de Sevilla. Downloaded on June 28,2022 at 11:08:41 UTC from IEEE Xplore. Restrictions apply.

UNIT CELLS WITH HIGHER SYMMETRIES

The description of a unit cell as a multiport network and transfer matrix is particularly helpful when dealing with geometrical symmetries present inside each unit cell. The case of glide and twist symmetries are considered in [19] and [55].

A glide-symmetric unit cell is invariant under a mirroring operation and a translation of a half of a period. In this case, the eigenproblem can be formulated by means of the transfer matrix of a half cell $[\hat{\mathbf{T}}]$ and a geometric diagonal matrix $[\mathbf{Q}]$:

$$[\hat{\mathbf{T}}]\begin{bmatrix}\mathbf{V}\\ \mathbf{I}\end{bmatrix} = e^{\gamma p/2}\begin{bmatrix}[\mathbf{Q}] & [\mathbf{0}]\\ [\mathbf{0}] & [\mathbf{Q}]\end{bmatrix}\begin{bmatrix}\mathbf{V}\\ \mathbf{I}\end{bmatrix}. \tag{S1}$$

The diagonal entries q_{ii} of $[\mathbf{Q}]$ describe the mirroring of each mode and are simply $q_{ii} = 1$ if the ith mode is even and $q_{ii} = -1$ if the ith mode is odd with respect to the mirroring direction. Note that in a 2D glide-symmetric case, the reduced unit cell is one quarter of a nonminimal unit cell obtained by a suitable rotation of the minimal one [19].

A twist-symmetric cell is invariant under a rotation of $2\pi/n$ and a translation of a period divided by n, with n being an integer. In this case, the problem can still be formulated as in (S1), with $[\hat{\mathbf{T}}]$ now being the transfer matrix of one nth of the period and $e^{\gamma p/n}$ replacing $e^{\gamma p/2}$.

Two equivalent choices are possible for the azimuthal dependence of the port modes: one can adopt either a basis of imaginary exponentials or of trigonometric functions. Let us assume that the ith mode at the ports of the unit cell has an imaginary exponential azimuthal variation of $e^{jn_i\varphi}$, with n_i being a suitable integer. In this case, the $[\mathbf{Q}]$ matrix is a diagonal matrix whose diagonal elements describe the rotation of each mode and are simply given by $q_{ii} = e^{jn_i 2\pi/n}$.

If the ith mode has a sinusoidal azimuthal variation of the kind $\cos(n_i\varphi)$ or $\sin(n_i\varphi)$, the $[\mathbf{Q}]$ matrix is a block diagonal matrix, whose blocks are defined as

$$[\mathbf{Q}_{ii}] = \begin{bmatrix}\cos\left(n_i\frac{2\pi}{n}\right) & \sin\left(n_i\frac{2\pi}{n}\right)\\ -\sin\left(n_i\frac{2\pi}{n}\right) & \cos\left(n_i\frac{2\pi}{n}\right)\end{bmatrix}. \tag{S2}$$

2D PERIODIC STRUCTURES

The multimode transfer-matrix method can be straightforwardly used for the study of 2D periodic structures [19]. As presented in Figure 4, the unit cell of this problem can be described as a region accessible through four geometrical faces, numbered from 1 to 4. Faces 1 and 2 are considered here as input faces and 3 and 4 as output faces. On each face, M modes can be defined as they were in the previous section. Each mode of each face is then associated with a port. In this way, the cell is associated with a $4M$-port network. Commercial software can easily extract the scattering matrix of this network as in (9), where each submatrix now has dimensions of $2M \times 2M$. More specifically, the 2D version of the submatrices in (9) can be written in the following block form where the couplings among the four different geometrical faces appear explicitly:

$$[\mathbf{S}_{ii}] = \begin{bmatrix}[\mathbf{S}_{11}] & [\mathbf{S}_{12}]\\ [\mathbf{S}_{21}] & [\mathbf{S}_{22}]\end{bmatrix} \qquad [\mathbf{S}_{io}] = \begin{bmatrix}[\mathbf{S}_{13}] & [\mathbf{S}_{14}]\\ [\mathbf{S}_{23}] & [\mathbf{S}_{24}]\end{bmatrix}$$
$$[\mathbf{S}_{oi}] = \begin{bmatrix}[\mathbf{S}_{31}] & [\mathbf{S}_{32}]\\ [\mathbf{S}_{41}] & [\mathbf{S}_{42}]\end{bmatrix} \qquad [\mathbf{S}_{oo}] = \begin{bmatrix}[\mathbf{S}_{33}] & [\mathbf{S}_{34}]\\ [\mathbf{S}_{43}] & [\mathbf{S}_{44}]\end{bmatrix}. \tag{24}$$

The transfer matrix can then be computed by using the same equations, that is, (11)–(14). This matrix operates a transformation from the output to the input ports as

$$\begin{bmatrix}\mathbf{V}_1\\ \mathbf{V}_2\\ \mathbf{I}_1\\ \mathbf{I}_2\end{bmatrix} = [\mathbf{T}]\begin{bmatrix}\mathbf{V}_3\\ \mathbf{V}_4\\ \mathbf{I}_3\\ \mathbf{I}_4\end{bmatrix}. \tag{25}$$

In 2D periodic structures, Floquet boundary conditions should be enforced along the two periodicity axes as $\mathbf{V}_3 = e^{-\gamma_x p_x}\mathbf{V}_1$ and $\mathbf{V}_4 = e^{-\gamma_y p_y}\mathbf{V}_2$ and, equivalently, for the currents (p_x and p_y, the periods along the x- and y-directions). From (25), these conditions can be formulated as the following eigenvalue problem:

$$[\mathbf{T}]\begin{bmatrix}\mathbf{V}_3\\ \mathbf{V}_4\\ \mathbf{I}_3\\ \mathbf{I}_4\end{bmatrix} = \begin{bmatrix}e^{\gamma_x p_x}\mathbf{V}_3\\ e^{\gamma_y p_y}\mathbf{V}_4\\ e^{\gamma_x p_x}\mathbf{I}_3\\ e^{\gamma_y p_y}\mathbf{I}_4\end{bmatrix} = [\mathbf{B}(\gamma_x p_x, \gamma_y p_y)]\begin{bmatrix}\mathbf{V}_3\\ \mathbf{V}_4\\ \mathbf{I}_3\\ \mathbf{I}_4\end{bmatrix}, \tag{26}$$

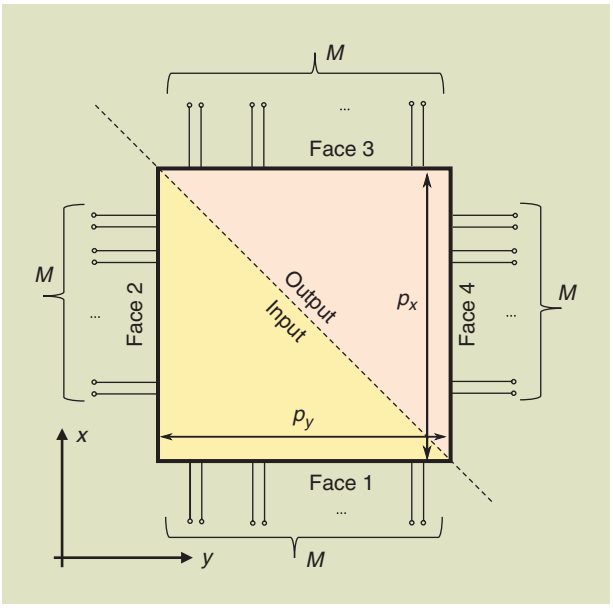

FIGURE 4. The top view of the unit cell of a 2D periodic structure with periodicity along the x- and y- directions. M modes are retained on each of the four geometrical faces.

Authorized licensed use limited to: Universidad de Sevilla. Downloaded on June 28,2022 at 11:08:41 UTC from IEEE Xplore. Restrictions apply.

where

$$[\mathbf{B}] = \begin{bmatrix} e^{\gamma_x p_x}[\mathbf{1}] & [\mathbf{0}] & [\mathbf{0}] & [\mathbf{0}] \\ [\mathbf{0}] & e^{\gamma_y p_y}[\mathbf{1}] & [\mathbf{0}] & [\mathbf{0}] \\ [\mathbf{0}] & [\mathbf{0}] & e^{\gamma_x p_x}[\mathbf{1}] & [\mathbf{0}] \\ [\mathbf{0}] & [\mathbf{0}] & [\mathbf{0}] & e^{\gamma_y p_y}[\mathbf{1}] \end{bmatrix}. \quad (27)$$

Unlike the eigenproblem in (17), the one in (26) is not linear and, in general, is expected to be solved numerically for the unknown complex phase shifts, $\gamma_x p_x$ and $\gamma_y p_y$. The right-hand side of (26) is brought to the left, thus obtaining an eigenvalue problem of the kind given in (2). The phase shifts can then be computed, in general, as the solution of

$$\det\{[\mathbf{T}(\omega)] - [\mathbf{B}(\gamma_x p_x, \gamma_y p_y)]\} = 0, \quad (28)$$

by means of an appropriate zero-searching algorithm. Fortunately, the transfer matrix $[\mathbf{T}(\omega)]$, which is the only part of (28) requiring the solution of a full-wave problem, has to be obtained only once at each frequency in this zero-searching process, which simplifies considerably the numerical procedure. In most cases, only a few cuts of the Brillouin diagram are required. For example, an irreducible zone of a unit-cell symmetric with respect to its center (namely, $p_x = p_y$) should be plotted along three spectral directions: 1) $\gamma_y = 0$, (26) is solved for $\gamma_x p_x$; 2) $\gamma_x p_x = \mathrm{j}\pi$, (26) is solved for $\gamma_y p_y$; and 3) $\gamma_x = \gamma_y$, (26) is solved for $\gamma_x p_x = \gamma_y p_y$. Although in these three cases there is only one unknown, only the last case leads to a standard, linear eigenvalue problem.

Finally, it is interesting to note that the multicell method [43]–[47], denoted here as method N-uc, cannot be directly extended to obtain the complete dispersion diagram of 2D periodic structures because at least four ports are required to define access to the unit cell (or, equivalently, to the N-cell system), and a 2×2 transfer matrix cannot describe all the possible propagation directions in this case. Actually, only the conditions of propagation along the principal axes of the structure could be satisfactorily implemented using the multicell method. This means that propagation along the x- and y-directions (having $k_y = 0$ and $k_x = 0$, respectively) can be implemented using a chain of N 2D unit cells along the same direction and by using periodic boundary conditions in the 2D unit cells at $y = 0$ or $x = 0$ and $y = P_y$ or $x = P_x$. However, propagation under any other condition (including $k_x = k_y$) is quite difficult to reproduce by a 1D chain of 2D unit cells. Also, it should be noted that the present multimodal method could be used in a similar way for the study of 3D periodic structures, although this case is beyond the scope of this article.

RESULTS

The multimode transfer-matrix method discussed in the previous section will be denoted in this section as the *HOM* method. This proposed methodology will be validated with a number of examples, including some novel periodic structures. Through these examples, we discuss some important practical issues to take into account during the method's implementation. One of the most important practical considerations concerning the suitable application of the method that we found is that, when computing the generalized scattering matrix with the full-wave EM simulator, the input/output ports should be located at planes of the unit cell, whose domain of definition ensures that the combination of the multiple modes at the input/output waveguide ports can account appropriately for the spatial variations caused by the discontinuities in these ports. This general rule for the location of the ports will lead to different port choices in the specific application cases to be discussed in this section.

Another important consideration concerns the number and type of modes to be set in the ports. Again, every specific structure under study will demand a previous analysis of the situation, although, again following the previous general rule, the choice of modes should be guided by the required spatial variations imposed by the discontinuities inside the unit cell. For instance, strong spatial variation along one of the transverse dimensions of the unit cell is a hint that some HOMs associated with this spatial direction would be required. These considerations have been applied in the following study cases, with the number of modes finally employed in each case being dictated by the good convergence of the values of the phase and attenuation constants.

The first validation example is the corrugated parallel-plate waveguide previously studied in [40, Fig. 6]. In that work, it was shown that, when the corrugations have glide symmetry and are electrically close, method 1-uc did not work well and method N-uc required at least five cells ($N = 5$) to match the CST results. If the present HOM method is now applied to a single unit-cell of the structure, then, by checking Figure 5, it can be determined that the phase shift ($\beta p/\pi$) given by this method is in very good agreement with the CST results when $M = 3$ modes are employed. The HOM method also provides the values of the attenuation constant (αp), which are different from zero only in the stopband between 13.7 and 14.7 GHz. Obtaining the attenuation constant in the stopband can be very relevant from a practical point of view because the small values of αp would lead to nonnegligible levels of transmission in finite

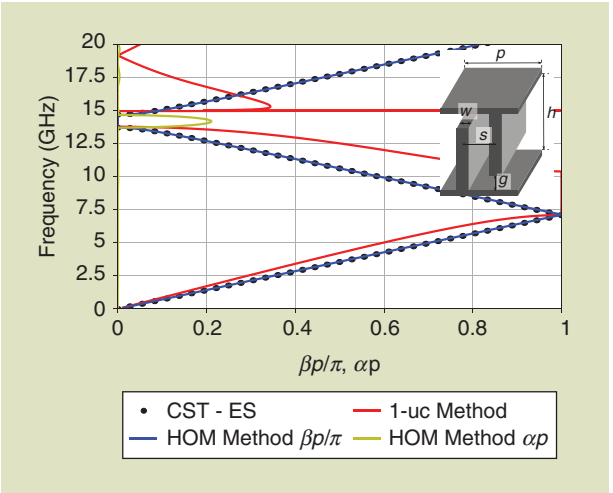

FIGURE 5. The dispersion diagram of a parallel-plate waveguide with corrugations having glide symmetry. The results from the HOM method are computed using $M = 3$ modes. The inset of the figure shows a cross view of the unit cell with dimensions $p = 6$, $h = 10$, $s = 2$, $w = 1$, and $g = 1$ mm.

Authorized licensed use limited to: Universidad de Sevilla. Downloaded on June 28,2022 at 11:08:41 UTC from IEEE Xplore. Restrictions apply.

periodic structures. Thus, for practical, finite periodic structures (made up of N unit cells), the stopband should be defined as that frequency band where αNp is beyond a certain threshold, for instance, $\alpha Np = \ln 10$, to ensure $|S_{21}| < -20$ dB.

For computing the generalized scattering matrix using the commercial simulator, the unit-cell geometry has been taken as shown in the inset in Figure 5. If the unit cell were to be defined with input/output ports at the center of the metal corrugations, the performance of the HOM method would be rather poor because the HOMs at the ports would hardly be congruent with the vertical variations caused by the corrugations in these ports. Also, because the present 1D case has no spatial variation along the transverse direction, the transverse electrical size of the unit cell has been made small and bounded by perfect magnetic walls. These last conditions will ensure that the modes in the ports resemble the modes of a parallel-plate waveguide.

The next structure to be analyzed is the 1D metal corrugated surface [6] shown in the inset of Figure 6. The phase shift of this structure computed by an HOM is found to be in good agreement with the values provided by CST as well as with the approximated formula in [6, eq. (7)–(22)]. The attenuation constant provided by the HOM method shows a partial agreement with the results provided by [6, eq. (7)–(22)], a fact that is somewhat expected due to the approximate nature of this expression [the values of $\alpha/(3k_0)$ are plotted in Figure 6 to fit the range of variation of the attenuation constant]. The HOM results are found to converge when five modes ($M = 5$) are used in the method, a fact that can be considered a test of self-consistency of the method. The CST values of the generalized scattering matrix for this structure were obtained with waveguide ports located in the groove of the corrugations. In our experience, and similar to the structure in Figure 5, the input/output ports should be located inside the groove, rather than in the middle of the corrugations. In the present open-boundary situation, the ports have to be a few times larger than the corrugations to correctly model the attenuation constant. For this specific case, we have considered a port that is four times the height of the corrugations.

A third example, displayed in Figure 7, is an LWA previously treated in [56] and consisting of a microstrip line periodically loaded with vertical central vias. In this kind of leaky-wave structure, obtaining the dispersion diagram for the attenuation constant is key for design purposes and, therefore, robust methods for its computation are of high practical relevance. The results of the HOM method are found to agree well with those provided by the IE method reported in [32] and the multiple-cell approach discussed in [56]. Only three HOMs are necessary to obtain a good convergence in the HOM method used in this structure. Note that the method accounts well for the proper and improper leaky-wave solutions shown in Figure 7 (additional details about these solutions are discussed in [32].)

A final 1D structure to be analyzed is the groove-gap waveguide structure presented in the inset of Figure 8. This waveguide was used as the underlying leakage system for the high-performance LWA reported in [58]. The structure is composed of a central waveguide region laterally bounded on the left by three rows of EM bandgap (EBG) pins and on the right by one row of leaky-wave pins that allow for radiation. The top and bottom perfect electric conductor plates shield the waveguide in the vertical direction. A preliminary study of the dispersion diagrams of the partial waveguides that make up this complete waveguide was shown in [57, Fig. 2]. Now, the complete waveguide unit cell is analyzed by means of the HOM method both in the case of transverse perfectly matched layers (PMLs), open in CST, and perfect magnetic conductor (PMC) boundary conditions. Only the results of this latter case

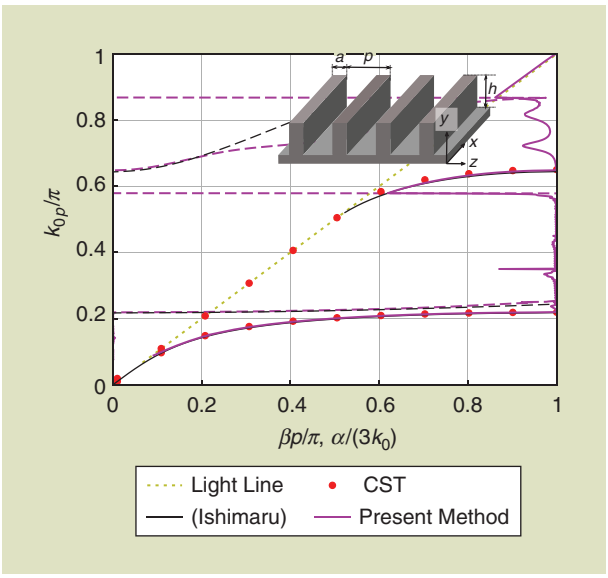

FIGURE 6. The dispersion diagram ($\beta p/\pi$: solid lines; $\alpha/(3k_0)$: dashed lines) of a 1D corrugated perfect-conductor surface. The dimensions are $a = 0.8$ and $h = 2\,p$. Our HOM data ($M = 5$) are compared with those of CST and with those in [6, eq. (7)–(22)].

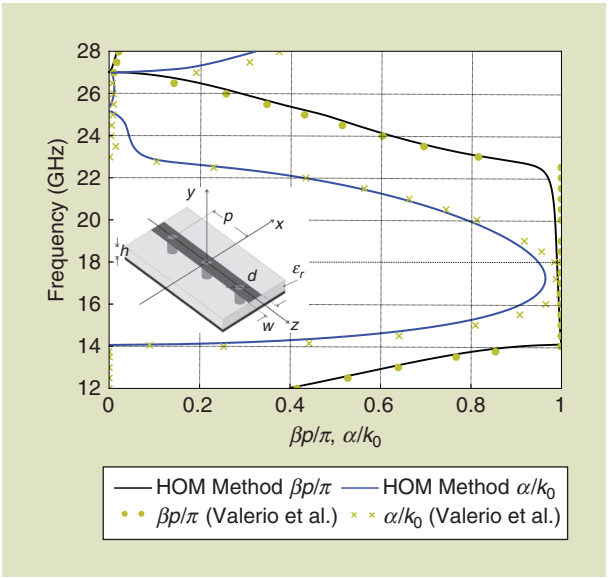

FIGURE 7. The dispersion diagram of a microstrip LWA with vertical vias already studied in [56, Fig. 10]. The HOM results have been obtained using three modes ($M = 3$).

Authorized licensed use limited to: Universidad de Sevilla. Downloaded on June 28,2022 at 11:08:41 UTC from IEEE Xplore. Restrictions apply.

are compared with those of the dispersion diagram computed using CST because the eigenmode solver of CST can only deal with shielded scenarios, as previously discussed in the "Periodic Structures" section.

The agreement for the phase shift of the CST results with the HOM-PMC results is very good, but these results are slightly different than the HOM-Open ones corresponding to the more realistic waveguide with open lateral conditions that now allows for radiation (key in this LWA structure). The attenuation constant of the leaky-wave waveguide is also depicted in Figure 8, and its values are found to converge when five modes ($M = 5$) are employed in the HOM method. The scattering parameters were obtained using the time-domain solver of CST with waveguide ports defined at the center of the pins. In this manner, CST provides the three first modes as those which can propagate through the EBG pins below the EBG frequencies, a fourth mode that mainly propagates in the leaky-wave pin, and a fifth mode that primarily propagates in the groove waveguide. The latter is the mode in which we are mainly interested in for this specific design. PML (open condition in CST) was defined at the right side of the leaky-wave pin to emulate a perfect radiation without reflections.

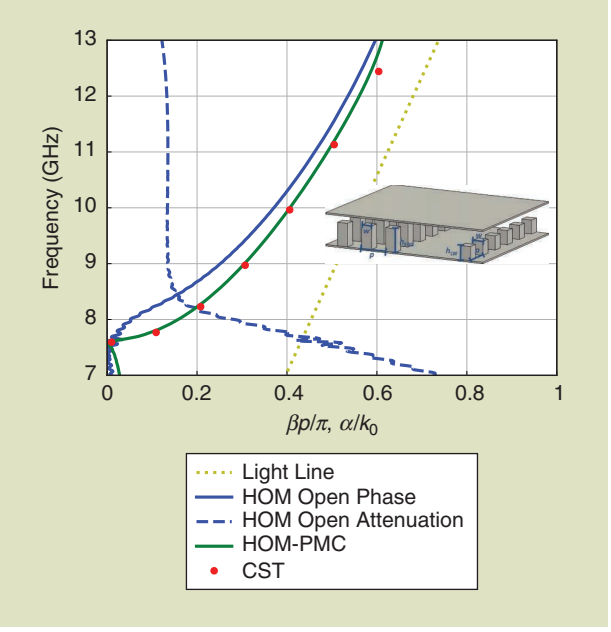

FIGURE 8. The dispersion diagram of the groove-gap waveguide studied in [57, Fig. 2]. The groove waveguide corresponds to the standard WR-90. The dimensions are $w = 3$, $p = 8.5$, $h_{LW} = 3.5$, and $h_{EBG} = 7.5$ mm. PMC: perfect magnetic conductor.

To confirm the versatility of the HOM approach when applied to 2D periodic structures, as described in the "2D Periodic Structures" section, two further 2D periodic structures are analyzed next. In Figure 9, the full dispersion diagram of a 2D periodic mushroom surface is shown [its corresponding unit cell is depicted in the inset of Figure 9(a)]. The structure was simulated with a metallic plate on the top; because the results concern bound modes, the diagram is not affected by the presence of this top plate as verified by varying its distance from the surface. Segment Γ-X shows the phase constant in the interval $0 \le \beta_x p_x \le \pi$ and $k_y = 0$, segment X-M shows the phase constant in the interval $0 \le \beta_y p_y \le \pi$ and $k_x p_x = \pi$, and segment M-Γ shows the phase constant in the interval $\pi \ge \beta_x p_x \ge 0$ and $k_x = k_y$. The phase shifts obtained with the HOM method (solid curves) are validated using the results from the CST eigenmode solver simulations (circles) when related to real modes, with a perfect agreement found in the entire frequency

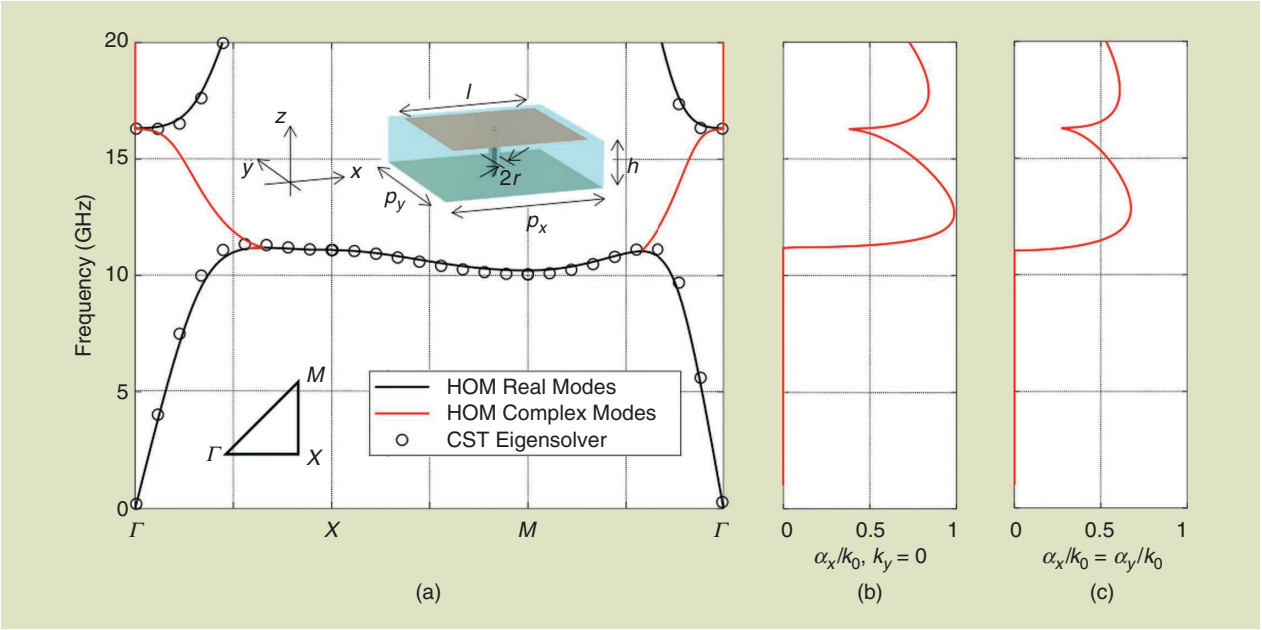

FIGURE 9. A 2D dispersion diagram of the mushroom metasurface is shown in the inset. $h = 1$, $p_x = p_y = 3.5$, $l = 3$, and $2r = 0.5$ mm with substrate $\varepsilon_r = 2.2$. (a) A phase-constant $\beta p/\pi$ in the irreducible Brillouin zone. The normalized attenuation constant α_x/k_0 with (b) $k_y = 0$ and (c) $k_y = k_x$.

Authorized licensed use limited to: Universidad de Sevilla. Downloaded on June 28,2022 at 11:08:41 UTC from IEEE Xplore. Restrictions apply.

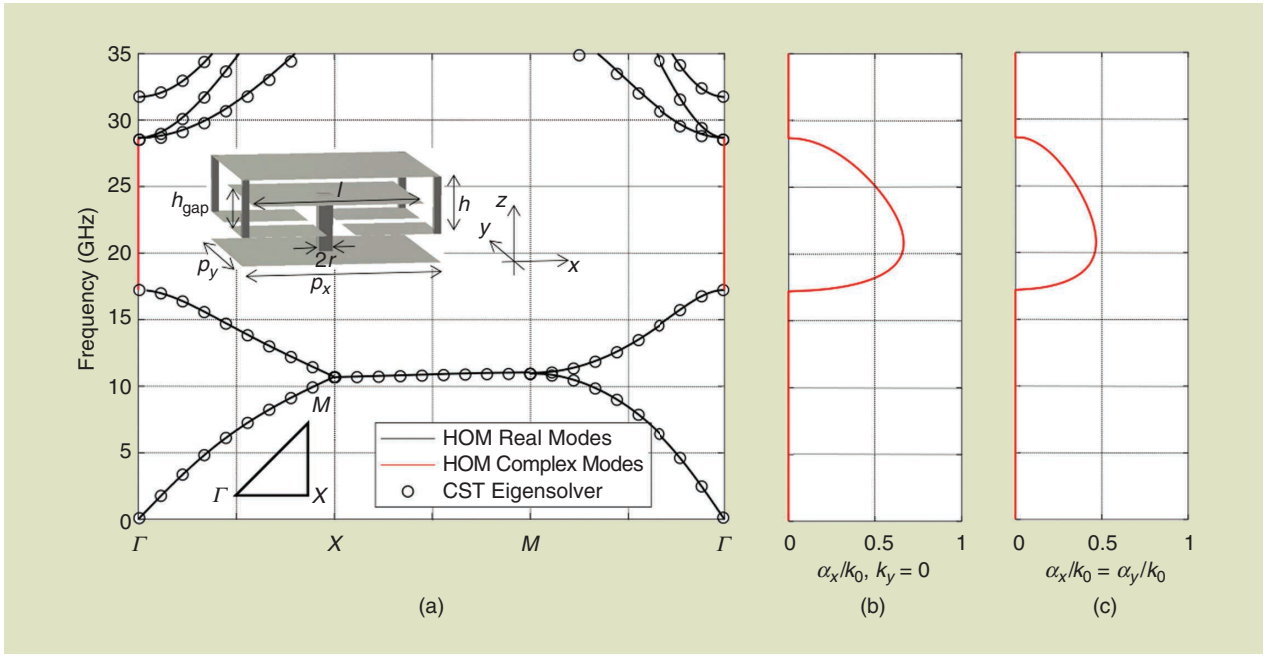

FIGURE 10. A 2D dispersion diagram of the glide-symmetric mushroom metasurface is shown in the inset. $h = 1$, $h_{gap} = 0.5$, $p_x = p_y = 3.5$, $l = 3$, and $2r = 0.5$ mm. No dielectric substrate is used. (a) Phase shift $\beta p/\pi$ in the irreducible Brillouin zone. Normalized attenuation constant α_x/k_0 with (b) $k_y = 0$ and (c) $k_y = k_x$.

range considered. The attenuation constants of complex modes, normalized to the free-space wavenumber, are shown in separate subfigures for each propagation direction. In the HOM analysis, $M = 9$ modes have been employed on each one of the four geometrical faces defined on the boundary of the unit cell to ensure convergence of the results shown in this article.

Concerning the Γ-X section of Figure 9(a), only the bound, real modes propagate up to 11.2 GHz along the x-direction of the surface (black line). At 11.2 GHz, two real modes merge into two complex conjugate modes [only one is shown in Figure 9(a) and (b) (red lines)]. The phase constant of the complex mode varies until 16.35 GHz, and then it becomes zero at higher frequencies, but its attenuation constant stays different from zero. These complex modes are not validated with CST because they cannot be recovered by the eigenmode solver tool. At 16.35 GHz, another higher-order real mode starts propagating along the x-direction. The X-M section of the diagram shows that when the propagation is studied along the y-direction with $k_x p_x = \pi$, only one real mode propagates between 10.05 and 11.1 GHz. Finally, the M-Γ section of Figure 9(a) shows the propagation along the diagonal of the unit cell, where $k_x = k_y$ and a similar behavior as the one along the x-direction are observed with a stopband from 11.08 to 16.47 GHz, where a complex mode is shown in red lines together with its attenuation constant.

The same analysis as in Figure 9 is performed in Figure 10 with two mushroom surfaces placed in a glide-symmetric configuration, i.e., mirrored with respect to a plane parallel to the surface and off-shifted half a period in both periodicity directions. Although 1D glide symmetry was first studied in the 1960s and 1970s [53], new applications have recently been found for 2D glide-symmetric periodic structures [59], [60]. As explained in [19], glide symmetry can strongly modify the dispersion properties of 2D periodic structures. The results in Figure 10 are again simulated with nine modes on each geometrical face and plotted in a 2D Brillouin diagram. As usual, the glide symmetry suppressed the stopband at the X point present in the previous nonglide case. Now a real mode is present up to 17.22 GHz, and a stopband arises this time at the Γ point between 17.22 and 28.52 GHz, where a complex mode has been found with the HOM method (and again, not validated with the CST eigenmode solver tool because complex modes cannot be recovered using it). At 28.52 GHz, two real modes start propagating, and at 31.72 GHz, another higher-order real mode starts propagating. These modes are also recovered using the CST eigenmode solver.

In the X-M propagation direction, one propagating mode is found. This mode has double multiplicity because it can be regarded as the merging of the two real branches reaching X coming from Γ. In the M-Γ section of Figure 10(a), a similar behavior as the one along the x-direction is observed, with the absence of a stopband at the M point, a complex mode responsible of a stopband between 17.4 and 28.4 GHz, and three higher-order modes that start propagating at 28.64 (two of them) and 31.72 GHz.

CONCLUSIONS

In this article, we described and discussed an efficient method to calculate the dispersion diagram of periodic structures by using the scattering simulations of a single unit-cell. More specifically, the diagram was obtained after postprocessing the scattering matrices computed with commercial software for an isolated, single unit-cell that is fed with two/four ports, which, in turn, are excited using multiple modes.

Authorized licensed use limited to: Universidad de Sevilla. Downloaded on June 28,2022 at 11:08:41 UTC from IEEE Xplore. Restrictions apply.

The main advantage of the method is that it can calculate both the phase and attenuation constants. In particular, the attenuation constant due to leaky modes and stopbands cannot be calculated with the eigenmode solver of commercial software. In fact, the only possible computational methods for the leaky-wave attenuation are 1) rigorous, source-free full-wave time- or frequency-domain solvers enforcing complex Floquet-conditions at the periodic boundaries; or 2) scattering simulations of multiple unit cells excited with one single mode, leading to a much longer computation time and, possibly, the loss of accuracy if the macrocell becomes very large.

The proposed method enabled a fast, accurate, and comprehensive calculation of this attenuation constant. We validated the method with 1D/2D, bounded/unbounded, and conventional/glide-symmetric periodic structures. We also provided some guidelines to overcome the possible errors and limitations of applying this method. Specifically, we identified that the location, number, and type of the modes when computing the scattering parameters in the commercial software are critical. In our experience, the following are some of the most relevant practical aspects to be considered:

- The position of the input/output ports has been chosen so that the unit cell is as symmetric as possible. In our experience, the most convenient choice is to locate the ports at the housing waveguide.
- In case of open structures, the height of the ports should be larger than the material structure to account for possible radiation leakage emanating from the structure. However, this height should not be too large to avoid the presence of higher modes related to the ports, which do not have any relevant role in the field behavior of the unit cell.
- The number and type of modes to be chosen in the waveguide ports should be selected, taking into account the geometrical configuration of the discontinuity inside the unit cell so that the spatial variations caused by this discontinuity at the waveguide ports locations can be well matched with the set of modes already imposed in the ports.

ACKNOWLEDGMENTS

This work was partly supported by the Spanish Ministerio de Ciencia, Innovaci'on y Universidades and European Union FEDER funds under project TEC2017-84724-P, the French National Research Agency under grant ANR-16-CE24-0030, the Vinnova project High-5 (2018-01522) under the Strategic Programme on Smart Electronic Systems, and the Stiftelsen Åforsk project H-Materials (18-302). The work of Francisco Mesa was also funded by the Spanish government (Salvador de Madariaga Fellowship PRX19/00025). The corresponding author is Oscar Quevedo-Teruel.

AUTHOR INFORMATION

Francisco Mesa (mesa@us.es) is currently a professor in the Departamento de Fisica Aplicada 1, Universidad de Sevilla. His research interests include electromagnetic propagation/radiation in planar structures. He is a Fellow of IEEE.

Guido Valerio (guido.valerio@sorbonne-universite.fr) is an associate professor at Sorbonne Université, CNRS, Laboratoire de Génie Electrique et Electronique de Paris and Université Paris-Saclay, CentraleSupélec, CNRS, Laboratoire de Génie Electrique et Electronique de Paris. He works on numerical methods for waves in complex structures, namely, periodic Green's function computation, multilayered structures, and dispersive properties of artificial surfaces. He is a Senior Member of IEEE.

Raúl Rodríguez-Berral (rrberral@us.es) is an associate professor in the Departamento de Fisica Aplicada 1, Universidad de Sevilla. His research interests include numerical and analytical techniques for analyzing and modeling periodic structures.

Oscar Quevedo-Teruel (oscarqt@kth.se) is an associate professor and director of the Master Programme in Electromagnetics Fusion and Space Engineering at the School of Electrical Engineering and Computer Science at KTH Royal Institute of Technology in Stockholm, Sweden. He has made scientific contributions to periodic structures possessing higher symmetries, transformation optics, lens antennas, metasurfaces, and leaky-wave antennas. He is a Senior Member of IEEE.

REFERENCES

[1] N. W. Ashcroft and N. D. Mermin, *Solid State Physics*. Orlando, FL: Harcourt, 1976.

[2] R. E. Collin, *Field Theory of Guided Waves*, 2nd ed. New York: Wiley, 1990.

[3] K. Kurokawa, *An Introduction to the Theory of Microwave Circuits*. New York: Academic, 1969.

[4] F. Xu, K. Wu, and W. Hong, "Equivalent resonant cavity model of arbitrary periodic guided-wave structures and its application to finite-difference frequency-domain algorithm," *IEEE Trans. Microw. Theory Techn.*, vol. 55, no. 4, pp. 697–702, 2007. doi: 10.1109/TMTT.2007.893670.

[5] D. G. Dudley, *Mathematical Foundations for Electromagnetic Theory*. New York: Wiley, 1994.

[6] A. Ishimaru, *Electromagnetic Wave Propagation, Radiation, and Scattering*. Englewood Cliffs, NJ: Prentice Hall, 1991.

[7] T. Rozzi, L. Pierantoni, and M. Farina, "Eigenvalue approach to the efficient determination of the hybrid and complex spectrum of inhomogeneous, closed waveguide," *IEEE Trans. Microw. Theory Techn.*, vol. 45, no. 3, pp. 345–353, 1997. doi: 10.1109/22.563332.

[8] M. J. Freire, F. Mesa, and M. Horno, "Excitation of complex and backward mode on shielded lossless printed lines," *IEEE Trans. Microw. Theory Techn.*, vol. 47, no. 7, pp. 1098–1105, 1999. doi: 10.1109/22.775442.

[9] T. Tamir and A. Oliner, "Guided complex waves. Part I: Fields at an interface," *Proc. Inst. Elect. Eng.*, vol. 110, no. 2, pp. 310–334, 1963. doi: 10.1049/piee.1963.0044.

[10] F. Mesa, D. Jackson, and M. Freire, "High frequency leaky-mode excitation on a microstrip line," *IEEE Trans. Microw. Theory Techn.*, vol. 49, no. 12, pp. 2206–2215, 2001. doi: 10.1109/22.971602.

[11] M. Tsuji, S. Matsumoto, H. Shigesawa, and K. Takiyama, "Guided-wave experiments with dielectric waveguides having finite periodic corrugation," *IEEE Trans. Microw. Theory Techn.*, vol. 31, no. 4, pp. 337–344, 1983. doi: 10.1109/TMTT.1983.1131494.

[12] H. K. Liu and T. L. Dong, "Propagation characteristics for periodic waveguide based on generalized conservation of complex power technique," *IEEE Trans. Microw. Theory Techn.*, vol. 54, no. 9, pp. 3479–3485, 2006. doi: 10.1109/TMTT.2006.880647.

[13] B. Bandlow, R. Schuhmann, G. Lubkowski, and T. Weiland, "Analysis of single-cell modeling of periodic metamaterial structures," *IEEE Trans. Magn.*, vol. 44, no. 6, pp. 1662–1665, 2008. doi: 10.1109/TMAG.2007.916037.

[14] Y. Weitsch and T. F. Eibert, "Periodically loaded waveguide analysis by propagating and evanescent mode superposition," in *Proc. European Microwave Conf. (EuMC 2009)*, Oct. 2009, pp. 1271–1274.

[15] F. Bongard, J. Perruisseau-Carrier, and J. R. Mosig, "Enhanced periodic structure analysis based on a multiconductor transmission line model and application to metamaterials," *IEEE Trans. Microw. Theory Techn.*, vol. 57, no. 11, pp. 2715–2726, 2009. doi: 10.1109/TMTT.2009.2032482.

[16] R. Islam, M. Zedler, and G. V. Eleftheriades, "Modal analysis and wave propagation in finite 2D transmission-line metamaterials," *IEEE*

Authorized licensed use limited to: Universidad de Sevilla. Downloaded on June 28,2022 at 11:08:41 UTC from IEEE Xplore. Restrictions apply.

Trans. Antennas Propag., vol. 59, no. 5, pp. 1562–1570, 2011. doi: 10.1109/TAP.2011.2123068.
[17] J. Naqui et al., "Common-mode suppression in microstrip differential lines by means of complementary split ring resonators: Theory and applications," *IEEE Trans. Microw. Theory Techn.*, vol. 60, no. 10, pp. 3023–3034, 2012. doi: 10.1109/TMTT.2012.2209675.
[18] Y. Weitsch and T. F. Eibert, "Modal series expansion of eigensolutions for closed and open periodic waveguides," *IEEE Trans. Antennas Propag.*, vol. 60, no. 12, pp. 5881–5889, 2012. doi: 10.1109/TAP.2012.2211320.
[19] M. Bagheriasl, O. Quevedo-Teruel, and G. Valerio, "Bloch analysis of artificial lines and surfaces exhibiting glide symmetry," *IEEE Trans. Microw. Theory Techn.*, vol. 67, no. 7, pp. 2618–2628, 2019. doi: 10.1109/TMTT.2019.2916821.
[20] A. F. Peterson, S. L. Ray, and R. Mittra, *Computational Methods for Electromagnetics*. New York: Wiley, 1997.
[21] R. F. Harrington, *Field Computation by Moment Methods*. New York: Wiley, 1993.
[22] J.-M. Jin, *The Finite Element Method in Electromagnetics*, 3rd ed. Hoboken, NJ: Wiley, 2014.
[23] R.-B. Hwang, *Periodic Structures: Mode-Matching Approach and Applications in Electromagnetic Engineering*. Hoboken, NJ: Wiley, 2012.
[24] M. S. Tong and W. C. Chew, *The Nystrom Method in Electromagnetics*. Hoboken, NJ: Wiley, 2019.
[25] D. M. Pozar, *Microwave Engineering*, 4th ed. New York: Wiley, 1990.
[26] G. Conciauro, M. Bressan, and C. Zuffada, "Waveguide modes via an integral equation leading to a linear matrix eigenvalue problem," *IEEE Trans. Microw. Theory Techn.*, vol. 32, no. 11, pp. 1495–1504, 1984. doi: 10.1109/TMTT.1984.1132880.
[27] P. Lampariello and R. Sorrentino, "The ZEPLS program for solving characteristic equations of electromagnetic structures (computer program descriptions)," *IEEE Trans. Microw. Theory Techn.*, vol. 23, no. 5, pp. 457–458, 1975. doi: 10.1109/TMTT.1975.1128598.
[28] M. A. Marin, S. Barkeshli, and P. H. Pathat, "On the location of proper and improper surface wave poles for the grounded dielectric slab (microstrip antennas)," *IEEE Trans. Antennas Propag.*, vol. 38, no. 4, pp. 1317–1324, 1990. doi: 10.1109/8.52278.
[29] R. Rodríguez-Berral, F. Mesa, and F. Medina, "Appropriate formulation of the characteristic equation for open nonreciprocal layered waveguides with different upper and lower half-spaces," *IEEE Trans. Microw. Theory Techn*, vol. 53, no. 5, pp. 1613–1623, 2005. doi: 10.1109/TMTT.2005.847051.
[30] P. Kowalczyk, "Global complex roots and poles finding algorithm based on phase analysis for propagation and radiation problems," *IEEE Trans. Antennas Propag.*, vol. 66, no. 12, pp. 7198–7205, 2018. doi: 10.1109/TAP.2018.2869213.
[31] G. P. Zouros, "CCOMP: An efficient algorithm for complex roots computation of determinantal equations," *Comput. Phys. Commun.*, vol. 222, pp. 339–350, Oct. 2018. doi: 10.1016/j.cpc.2017.09.023.
[32] P. Baccarelli, C. D. Nallo, S. Paulotto, and D. R. Jackson, "A full-wave numerical approach for modal analysis of 1-D periodic microstrip structures," *IEEE Trans. Microw. Theory Techn.*, vol. 54, no. 4, pp. 1350–1362, 2006. doi: 10.1109/TMTT.2006.871353.
[33] P. Harms, R. Mittra, and W. Ko, "Implementation of the periodic boundary condition in the finite-difference time-domain algorithm for FSS structures," *IEEE Trans. Antennas Propag.*, vol. 42, no. 9, pp. 1317–1324, 1994. doi: 10.1109/8.318653.
[34] M. Celuch-Marcysiak and W. K. Gwarek, "Spatially looped algorithms for time-domain analysis of periodic structures," *IEEE Trans. Microw. Theory Techn.*, vol. 43, no. 4, pp. 860–865, 1995. doi: 10.1109/22.375235.
[35] M. Chen, B. Houshmand, and T. Itoh, "FDTD analysis of a metal-strip-loaded dielectric leaky-wave antenna," *IEEE Trans. Antennas Propag.*, vol. 45, no. 8, pp. 1294–1301, 1997. doi: 10.1109/8.611250.
[36] T. Kokkinos, C. D. Sarris, and G. V. Eleftheriades, "Periodic FDTD analysis of leaky-wave structures and applications to the analysis of negative-refractive-index leaky-wave antennas," *IEEE Trans. Microw. Theory Techn.*, vol. 54, no. 4, pp. 1619–1630, 2006. doi: 10.1109/TMTT.2006.871367.
[37] N. Marcuvitz, *Waveguide Handbook*. New York: McGraw-Hill, 1951.
[38] G. Valerio, Z. Sipus, A. Grbic, and O. Quevedo-Teruel, "Accurate equivalent-circuit descriptions of thin glide-symmetric corrugated metasurfaces," *IEEE Trans. Antennas Propag.*, vol. 65, no. 5, pp. 2695–2700, 2017. doi: 10.1109/TAP.2017.2677923.
[39] S. Amari, R. Vahldieck, J. Bornemann, C. Forces, and C. Angel, "Accurate analysis of periodic structures with an additional symmetry in the unit cell from classical matrix eigenvalues," *IEEE Trans. Microw. Theory Techn.*, vol. 46, no. 10, pp. 1513–1515, 1998. doi: 10.1109/22.721158.
[40] F. Mesa, R. Rodríguez-Berral, and F. Medina, "On the computation of the dispersion diagram of symmetric one-dimensionally periodic structures," *Symmetry*, vol. 10, no. 8, p. 307, 2018. doi: 10.3390/sym10080307.
[41] M. Bozzi, S. Germani, L. Minelli, L. Perregrini, and P. de Maagt, "Efficient calculation of the dispersion diagram of planar electromagnetic band-gap structures by the MoM/BI-RME method," *IEEE Trans. Antennas Propag.*, vol. 53, no. 1, pp. 29–35, 2005. doi: 10.1109/TAP.2004.840522.
[42] J. E. Varela and J. Esteban, "Analysis of laterally open periodic waveguides by means of a generalized transverse resonance approach," *IEEE Trans. Microw. Theory Techn.*, vol. 59, no. 4, pp. 816–826, 2011. doi: 10.1109/TMTT.2011.2111379.
[43] M. Kahrizi, T. K. Sarkar, and Z. A. Maricevic, "Dynamic analysis of a microstrip line over a perforated ground plane," *IEEE Trans. Microw. Theory Techn.*, vol. 42, no. 5, pp. 820–825, 1994. doi: 10.1109/22.293530.
[44] L. Zhu, "Guided-wave characteristics of periodic coplanar waveguides with inductive loading-unit-length transmission parameters," *IEEE Trans. Microw. Theory Techn.*, vol. 51, no. 10, pp. 2133–2138, 2003. doi: 10.1109/TMTT.2003.817435.
[45] Y. C. Chen, C. K. C. Tzuang, T. Itoh, and T. K. Sarkar, "Modal characteristics of planar transmission lines with periodical perturbations: Their behaviors in bound, stopband, and radiation regions," *IEEE Trans. Antennas Propag.*, vol. 53, no. 1, pp. 47–58, 2005. doi: 10.1109/TAP.2004.840536.
[46] M. Bozzi, M. Pasian, L. Perregrini, and K. Wu, "On the losses in substrate-integrated waveguides and cavities," *Int. J. Microw. Wirel. Technol.*, vol. 1, no. 5, pp. 395–401, 2009. doi: 10.1017/S1759078709990493.
[47] G. Valerio, S. Paulotto, P. Baccarelli, P. Burghignoli, and A. Galli, "Accurate Bloch analysis of 1-D periodic lines through the simulation of truncated structures," *IEEE Trans. Antennas Propag.*, vol. 59, no. 6, pp. 2188–2195, 2011. doi: 10.1109/TAP.2011.2143667.
[48] A. Morini and T. Rozzi, "On the generalized scattering matrix of a lossless multiport," *IEEE Trans. Microw. Theory Techn.*, vol. 49, no. 1, pp. 160–165, 2001. doi: 10.1109/22.899987.
[49] J. A. Dobrowlski, *Microwave Network Design Using the Scattering Matrix*. Englewood Cliffs, NJ: Artech House, 2010.
[50] J. Frei, X.-D. Cai, and S. Muller, "Multiport S-parameter and T-parameter conversion with symmetry extension," *IEEE Trans. Microw. Theory Techn.*, vol. 56, no. 11, pp. 2493–2504, 2008. doi: 10.1109/TMTT.2008.2005873.
[51] J. Shekel, "Matrix analysis of multi-terminal transducers," *Proc. IRE*, vol. 42, no. 5, pp. 840–847, 1954. doi: 10.1109/JRPROC.1954.274523.
[52] T. Reveyrand, "Multiport conversions between S, Z, Y, h, ABCD, and T parameters," in *Proc. 2018 Int. Workshop Integrated Nonlinear Microwave and Millimetre-wave Circuits (INMMIC)*, pp. 1–3. doi: 10.1109/INMMIC.2018.8430023.
[53] A. Hessel, M. H. Chen, R. C. Li, and A. A. Oliner, "Propagation in periodically loaded waveguides with higher symmetries," *Proc. IEEE*, vol. 61, no. 2, pp. 183–195, 1973. doi: 10.1109/PROC.1973.9003.
[54] F. Ghasemifard, M. Norgren, and O. Quevedo-Teruel, "Twist and polar glide symmetries: An additional degree of freedom to control the propagation characteristics of periodic structures," *Sci. Rep.*, vol. 8, no. 1, p. 11266, July 2018. doi: 10.1038/s41598-018-29565-6.
[55] M. Bagheriasl and G. Valerio, "Bloch analysis of electromagnetic waves in twist-symmetric lines," *Symmetry*, vol. 11, no. 5, pp. 1–11, 2019. doi: 10.3390/sym11050620.
[56] G. Valerio et al., "Efficient computation of 1-D periodic layered mixed potentials for the analysis of leaky-wave antennas with vertical elements," *IEEE Trans. Antennas Propag.*, vol. 63, no. 6, pp. 2396–2411, 2015. doi: 10.1109/TAP.2015.2412959.
[57] L. Wang, J. L. Gomez-Tornero, E. Rajo-Iglesias, and O. Quevedo-Teruel, "Low-dispersive leaky-wave antenna Integrated in groove gap waveguide technology," *IEEE Trans. Antennas Propag.*, vol. 66, no. 11, pp. 5727–5736, 2018. doi: 10.1109/TAP.2018.2863115.
[58] M. Vukomanovic, J. Vazquez-Roy, O. Quevedo-Teruel, E. Rajo-Iglesias, and Z. Sipus, "Gap waveguide leaky-wave antenna," *IEEE Trans. Antennas Propag.*, vol. 64, no. 5, pp. 2055–2060, May 2016. doi: 10.1109/TAP.2016.2539376.
[59] M. Ebrahimpouri, E. Rajo-Iglesias, Z. Sipus, and O. Quevedo-Teruel, "Cost-effective gap waveguide technology based on glide-symmetric holey EBG structures," *IEEE Trans. Microw. Theory Techn.*, vol. 66, no. 2, pp. 927–934, Feb. 2018. doi: 10.1109/TMTT.2017.2764091.
[60] O. Quevedo-Teruel, J. Miao, M. Mattsson, A. Algaba-Brazalez, M. Johansson, and L. Manholm, "Glide-symmetric fully metallic Luneburg lens for 5G communications at Ka-band," *IEEE Antennas Wirel. Propag. Lett.*, vol. 17, no. 9, pp. 1588–1592, Sept. 2018. doi: 10.1109/LAWP.2018.2856371.

Authorized licensed use limited to: Universidad de Sevilla. Downloaded on June 28,2022 at 11:08:41 UTC from IEEE Xplore. Restrictions apply.